Published in final edited form as:

Nature. 2010 January 14; 463(7278): 250–254. doi:10.1038/nature08671.

STRUCTURAL BASIS FOR THE PHOTOCONVERSION OF A PHYTOCHROME TO THE ACTIVATED FAR-RED LIGHT-ABSORBING FORM

Andrew T. Ulijasz[1,†], **Gabriel Cornilescu**[2,†], **Claudia C. Cornilescu**[2], **Junrui Zhang**[1], **Mario Rivera**[3], **John L. Markley**[2], and **Richard D. Vierstra**[1,*]

[1]Department of Genetics, University of Wisconsin-Madison, Madison, WI 53706

[2]National Magnetic Resonance Facility at Madison, University of Wisconsin-Madison, Madison, WI 53706

[3]Multidisciplinary Research Building, University of Kansas, Lawrence, KS 66057-1620

Abstract

Phytochromes are a collection of bilin-containing photoreceptors that regulate numerous photoresponses in plants and microorganisms through their ability to photointerconvert between a red light-absorbing, ground state Pr and a far-red light-absorbing, photoactivated state Pfr1,2. While the structures of several phytochromes as Pr have been determined3-7, little is known about the structure of Pfr and how it initiates signaling. Here, we describe the three-dimensional solution structure of the bilin-binding domain as Pfr using the cyanobacterial phytochrome from *Synechococcus* OSB'. Contrary to predictions, light-induced rotation of the A but not the D pyrrole ring is the primary motion of the chromophore during photoconversion. Subsequent rearrangements within the protein then affect intra- and interdomain contact sites within the phytochrome dimer. From our models, we propose that phytochromes act by propagating reversible light-driven conformational changes in the bilin to altered contacts between the adjacent output domains, which in most phytochromes direct differential phosphotransfer.

The biological perception of light is mediated by a collection of photoreceptors that couple light absorption to specific signaling cascades. One influential set is the phytochromes, a superfamily of dimeric chromoproteins that absorb light via a bound bilin (or linear

*To whom correspondences should be addressed at the Department of Genetics, 425-G, Henry Mall, University of Wisconsin-Madison, Madison, Wisconsin 53706 USA, Vierstra@wisc.edu.

†Both authors contributed equally to this work.

Author Contributions. R.D.V. and A.T.U. initiated the collaboration. A.T.U and J.Z. purified the chromoproteins and A.T.U. characterized the samples. M.R. provided the isotopically labeled ALA. G.C. collected the NMR spectra and solved the NMR structures with C.C.C. and J.L.M. All authors interpreted the 3-D structures. R.D.V, A.T.U, C.C.C and G.C prepared the manuscript, tables, and figures.

Author Information. Atomic coordinates and structures have been deposited in the Protein Data Bank under accession code 2KOI for Pr and 2KLI for Pfr. Reprints and permission information is available at npg.nature.com/reprintsandpermissions. The authors declare no competing financial interests.

Full Methods and any associated references are available in the online version of the paper at www.nature.com/nature.

Supplementary Information is linked to the online version of the paper at www.nature.com/nature.

tetrapyrrole) chromophore1,2,8. The bilin is buried within an N-terminal cGMP phosphodiesterase/adenyl cyclase/FhlA (GAF) domain whose contacts with the chromophore generate much of the unique photochromic behavior of Phys. Typically, the GAF domain is preceded by a Per/Arndt/Sim (PAS) domain and followed by a Phy-associated (PHY) domain and an output module, which often includes a histidine kinase domain that initiates a two-component phosphorelay. By photointerconversion between Pr and Pfr, phytochromes act as light-regulated switches for measuring the fluence, direction, duration and color of the ambient light environment8.

Despite intensive study, we know little about how phytochromes acquire their unique photochromic behavior and how Pfr then initiates signal transmission. Recently, we and others provided important insights by determining the structure of the bilin-binding photosensory domain as Pr3-7. These models showed that the bilin is cradled within the GAF domain crevice, revealed a figure-of-eight knot that connects the PAS and GAF domains, identified a dimerization contact between adjacent GAF domains in the homodimer, and discovered a hairpin projection from the PHY domain that helps seal the chromophore pocket from the solvent. Unfortunately, these models have not fully illuminated how Pfr is generated. A long held notion is that the initial photochemistry involves a *Z* to *E* isomerization of the C15=C16 methine bridge which concomitantly rotates the D pyrrole ring9-13. Specific protein conformational changes have also been proposed from the structural analyses of an unusual phytochrome variant that prefers Pfr as the ground state, but whether these movements pertain to canonical phytochromes remains speculative7,14.

To better understand photoconversion, we used NMR spectroscopy to generate companion high resolution Pr and Pfr structures of the GAF domain from the phytochrome *SyB*-Cph1 obtained from the thermotolerant cyanobacterium *Synechococcus* OSB'. This fragment efficiently assembles with its native chromophore phycocyanobilin (PCB) to generate a chromoprotein with near full Pr/Pfr photochromicity4,15. NMR spectra were collected without illumination with the chromoprotein as Pr and during continuous red light irradiation, which produced an equimolar mixture of Pr and Pfr. By comparing the results to our previous *SyB*-Cph1(GAF) Pr structure4, we generated a highly refined solution structure of Pfr (Protein Data Bank (PDB) code 2KLI) and an improved solution structure of Pr (PDB code 2KOI) with structured backbone root mean square deviations of 0.44 Å and 0.30 Å, respectively.

The backbone conformation of the *SyB*-Cph1 GAF domain as Pfr is similar to that as Pr, indicating that the overall shape of this domain does not change dramatically during photoconversion (Fig. 1). However, photoinduced movements were obvious for the bilin and a number of amino acid side chains. In contrast to our previous report4, the refined Pr structure showed that the PCB A pyrrole ring is nearly perpendicular to the B and C rings, with the A-ring carbonyl now pointing away from the thioether linkage to Cys138 (Fig. 2a,b). Upon photoconversion to Pfr, the orientations of the B, C and D rings are unchanged. Instead, we found in the ensemble of Pfr conformers that the A ring becomes nearly co-planar with the B and C rings, implying a ~90° rotation around the C4=C5 bridge during photoconversion (Fig. 2b). The thioether linkage to PCB is also contorted, which is

supported by the fact that the Cys138 β carbon displays the largest chemical shift change during photoconversion (-4.6 ppm (Suppl. Fig. 1)). Most NMR signals from PCB exhibited considerable broadening in Pfr, suggesting increased mobility relative to the more rigid Pr state (Fig. 2c,d and Suppl. Fig. 2).

Although prior studies proposed that the D ring rotates during phototransformation9-11,13, our NMR analyses of *SyB*-Cph1(GAF) failed to detect significant chemical shift changes for this ring during photoconversion. For example, various NMR spectra for the D-ring $C17^1$ and $C18^2$ methyls, amide, the pyrrole nitrogen, and C18 failed to detect Pfr signals distinct from Pr, nor did the immediate neighboring $C13^1$ methyl of the C ring, whereas differences in and around the environment of the A ring were obvious (Fig. 2c,d, Suppl. Fig. 2, and ref. 15).

Rotation of the A ring of *SyB*-Cph1(GAF) is accompanied by conformational changes of several amino acids proximal to PCB, including Asp86, Tyr142, Phe82, Tyr54, His139, His169, Arg101 and Val100. Previous structural studies of Pr showed that the $N^{\delta 1}$ nitrogen of His139 contributes to a complex hydrogen bond network, involving the A-C ring nitrogens and a centrally positioned pyrrole water which together participate in the protonation cycle of the bilin during photoconversion, whereas the $N^{\psi 1}$ nitrogen of His169 hydrogen bonds with the C19 carbonyl oxygen to stabilize the D ring4-6,16,17. In Pfr, both these interactions are disrupted; the imidazole rings of His139 and His169 are rotated away from the pyrrole water and the D ring, respectively (Fig 3a-c). The position of His169 in Pfr is stabilized by displacement of strand β6 toward strand β1, leading to the formation of a new set of hydrogen bonds involving His170 with Tyr176 and Thr48 (Suppl. Fig. 3). Collectively, these changes likely alter the environment of the pyrrole water and thus the bilin photocycle16-19, a possibility supported by our observations that the Pfr forms of Tyr176-Phe, His169-Ala, and Thr48-Ala mutants thermally revert more rapidly back to Pr (Suppl. Fig. 4).

A second set of rearrangements during photoconversion involves Phe82, Tyr54, Asp86, and Tyr142 near the A and D rings of PCB (Figs. 3a-c and 4a,b). The Phe82 aromatic ring rotates ~30° to assume a parallel displaced orientation relative to the PCB D ring that could enable hydrophobic π stacking interactions (Fig. 4e,f). Movement of Phe82 eliminates a hydrogen bond between its main chain nitrogen and the hydroxyl of Tyr54, a conserved residue that helps avoid non-productive fluorescence of some Phys during photoexcitation15,16,20. Mutant analysis shows that both Phe82 and Tyr54 are required for Pfr formation and stability (Suppl. Fig. 4). Rotation of the A-ring nitrogen to its position in Pfr is stabilized by a new hydrogen bond with the main chain oxygen of Asp86. Subsequent motion of the Asp86 side chain then leads to a new hydrogen bond network with the hydroxyl of Tyr142 and the D-ring carbonyl, the importance of which is confirmed by the aberrant photochemistry of a Tyr142-Phe mutant and several Asp86 substitutions (Suppl. Fig. 4 and ref.15). Collectively, these movements help stabilize the D ring (in addition to its contact with Lys52), and decrease the solvent accessibility of the Pfr chromophore (Fig 4c,d). Given that the carboxylate group of Asp86 is predicted to form a double salt bridge with a conserved arginine located in the PHY domain hairpin3,7, movement of Asp86 likely affects this contact as well.

Perhaps the most dramatic change in the *SyB*-Cph1(GAF) domain during photoconversion involves movement of Arg101 (Fig. 3d-f). In Pr, Arg101 forms a double salt bridge with the carboxylate of the B-ring propionate, but in Pfr, strand β4 is disrupted, and Arg101 and Val100 swivel approximately 180° to encourage a salt bridge between Arg101 and Glu185 in helix α5 (Fig. 3d-f and Suppl. Fig. 5). Concomitant with this rotation is a 2.6 Å displacement of helix α2 toward the B-ring propionate, thus allowing Phe95 to fill the void left by Arg101. Previous mutagenic analyses of Arg101 and a comparable Arg in Arabidopsis PhyB revealed a critical role for this residue in Pfr stability and signaling4,22, whereas mutagenic studies of both Gln185 and Arg101 support the importance of their contact in Pfr (Suppl. Fig. 4). For example, the Gln185-Ala and Gln185-Glu mutants of *SyB*-Cph1 thermally revert from Pfr to Pr slower than wild type, whereas the Gln185-Arg and Arg101-Ala mutants revert much faster, with the Gln185-Arg mutant also displaying aberrant absorption spectra. Collectively, the new Pfr contact between Arg101 and Gln185 appears to adjust the position and/or flexibility of helix α5, as detected by notable chemical shift changes for several neighboring residues (*e.g.* Val184) and the unusual absence of NMR signals in Pfr from helix α5 (*e.g.*, Gln178, Glu179, Glu180, Leu181, and Gln185), which participates in Phy dimerization6,7.

Taken together, the structural differences between Pr and Pfr in *SyB*-Cph1(GAF) combined with the photochemical importance of a number of key conserved residues (Suppl. Fig. 6) offer a possible model for phytochrome photoconversion. An unexpected feature is the substantial rotation of the A ring, presumably driven by a C4=C5 isomerization, and a contortion of its thioether linkage to the protein instead of the former proposal that the D ring rotates9-13. Either isomerization or relaxation of the strained C4=C5 bridge during Pfr formation could account for the red-shifted absorption spectrum of Pfr by increasing the coupling of the π-conjugation system. Further red-shifting by π-stacking interactions with aromatic residues neighboring the D ring could help explain the Pfr/Pr chemical shift differences reported previously for the D ring23. Rotation of the A ring is also supported by photochemical studies with sterically locked bilins24,25 and by prior NMR spectra of phytochrome fragments also containing the PAS and PHY domains26,27, which strongly suggest that our results with *SyB*-Cph1(GAF) are not unique to this phytochrome nor artifactually generated by analysis of just the GAF domain. We note that the x-ray crystallographic structures of several Phys as Pr3-5,7,28 have modeled with a more coplanar configuration for the A ring relative to the B and C rings than seen here for *SyB*-Cph1 in solution. These differences could reflect subtle variations among Phys, inherent differences in the environment of the chromophore in crystals versus in solution, and/or radiation-induced damage of the Pr bilin during x-ray data collection that could relax the strain of a non-planar A ring5,28.

We propose that, subsequent to rotation of the A ring, a series of reversible conformational movements occur within the bilin-binding pocket that support the deprotonation/protonation cycle of the bilin, stabilize the Pfr form, and finally adjust several contact sites on the surface of the GAF domain. In particular, movement of the Asp86 and Tyr142 pair could affect the non-covalent interaction of the PHY domain with the GAF domain through its hairpin projection, which could then reorient by a hinge mechanism these domains relative

to each other. The swivel of Arg101 to contact Gln185 concomitantly reorients and/or destabilizes helix α5. Given the role of helix α5 in helping sister phytochromes dimerize and in covalently connecting the GAF and PHY domains3,6,7, even a subtle movement/unfolding of this helix might have profound consequences on intermolecular GAF/GAF dimerization and intramolecular GAF/PHY contacts.

Taken together, it is conceivable that such light-induced rearrangements then initiate a cascade of events within the phytochrome dimer that reorient the C-terminal output modules relative to each other and to the photosensory modules. For phytochromes bearing histidine kinase output modules, such light-driven rearrangements could then alter autophosphorylation *in trans* across the phytochrome dimer. In this manner, phytochromes may resemble the phototropin family of photoreceptors, which couples flavin photochemistry to selective destabilization of a helical contact adjacent to the photosensory domain and finally to activation of the appended output kinase29. Because the PYP family of photoreceptors may work by a similar light-triggered conformational switch30, our model for phytochromes provides further support for the notion that light-induced conformational changes are fundamental for photoactivated signaling.

METHODS SUMMARY

The GAF domain of *Synechococcus OSB*' Cph1 bearing a C-terminal 6His tag was expressed and assembled with PCB in *Escherichia coli* and purified as described previously4,15. The protein moiety was uniformly labeled by using expression medium containing $^{15}NH_4Cl$ and [^{13}C]-glycerol and an excess of unlabelled bilin precursor α-aminolevulinic acid (ALA). PCB was selectively labeled by adding [*U*-^{15}N]-ALA, [3-^{13}C]-ALA, [4-^{13}C]-ALA, [1,2-^{13}C]-ALA, or [*U*-^{15}N;*U*-^{13}C]-ALA to the medium. NMR spectra were collected with a ~50:50 equilibrium mixture of Pr and Pfr that was obtained by continuously irradiating the samples with red light15. Three-dimensional structures of Pr and Pfr were generated by a suite of NMR analyses using the prior model of *SyB*-Cph1(GAF) as a reference (PDB code 2K2N)4. Statistical support for the Pfr structure is present in Suppl. Table 1. The structures are also supported by the photochemical analyses of various *SyB*-Cph1(GAF-PHY) mutants generated by site-directed mutagenesis (Suppl. Fig. 4).

Supplementary Material

Refer to Web version on PubMed Central for supplementary material.

Acknowledgements

We thank Drs. Katrina Forest and W. Milo Westler for technical advice. This work was supported by a grant from the U.S. National Science Foundation (R.D.V.) and a postdoctoral fellowship from the American Heart Association (A.T.U.). C.C.C. was supported by the U.S National Institute of Health. This study was a collaboration with the National Magnetic Resonance Facility at Madison, which is supported by the U.S. National Institute of Health.

Appendix

METHODS

Chromoprotein production

The first 200 amino acids of *Synechococcus OSB'* (*SyB*) Cph1 bearing a C-terminal 6His tag were expressed, assembled with PCB in *Escherichia coli*, and purified using the dual-plasmid recombinant system described previously31,32. Even with its lack of an N-terminal PAS domain, *SyB*-Cph1 shares a number of photochemical properties with other members of the phytochrome superfamily, including red/far-red light photochromicity, the preference of Pr as the ground state, the extended configuration of the bilin in Pr, the protonation of the bilin as both Pr and Pfr, a similar fold of its GAF domain, and the importance of conserved amino acids lining the bilin-binding pocket31,32. Samples used for backbone, sidechain, and nuclear Overhauser effect (NOE) data collection were expressed in medium containing $^{15}NH_4Cl$ and [^{13}C]-glycerol and excess of the bilin precursor α-aminolevulinic acid (ALA) unlabeled. PCB was selectively labeled by adding [*U*-^{15}N]-ALA, [3-^{13}C]-ALA, [4-^{13}C]-ALA, [1,2-^{13}C]-ALA, or [*U*-^{15}N;*U*-^{13}C]-ALA (Sigma, St. Louis, MO) to the medium containing unlabeled NH_4Cl and glycerol.

Various site-directed mutants affecting the GAF-PHY fragment of *SyB*-Cph1 (residues 1-421) bearing a C-terminal 6His tag were generated by the QuickChange method (Stratagene, La Jolla, CA). PCB incorporation was assayed by zinc-induced fluorescence of the chromoproteins following SDS-PAGE32. The zinc-impregnated gels were irradiated with 260 nm light with the fluorescence emission detected in the visible region of the light spectrum. Pr and Pfr absorption and difference spectra, and rates of Pfr to Pr thermal reversion were measured at 55 °C as previously described32.

NMR Data Collection

For Pfr data collection of the *SyB*-Cph1(GAF) sample, an equilibrium mixture of Pr and Pfr was obtained by irradiating the Shigemi microcell solution with saturating red light and then maintaining this equilibrium during data collection by continuous irradiation with low fluence red light as described32. Unless noted otherwise, all NMR spectra were recorded on 800 and 600 MHz Varian INOVA spectrometers equipped with cryogenic probes. Samples used for backbone, sidechain, and nuclear Overhauser effect (NOE) experiments contained 1.7 mM [*U*-^{15}N;*U*-^{13}C]-*SyB*-Cph1(GAF) assembled with unlabelled PCB in 10 mM deuterated Tris-HCl (pH 8.5) and 0.03% NaN_3 in 93% H_2O/7% D_2O. Protein $^1D_{NH}$ and $^1D_{C\alpha H\alpha}$ residual dipole couplings (RDCs) were recorded with 1 mM [*U*-^{15}N;*U*-^{13}C]-*SyB*-Cph1(GAF) in anisotropic medium containing an axially stretched (5.4 mm to 4.2 mm) negatively charged acrylamide gel33 or supplemented with sodium dodecylsulfate-doped ditetradecyl-phosphatidylcholine/dihexyl-phosphatidylcholine bicelles (molar ratio 1:30:10^{10}). PCB 3-D ^{13}C NOE data and isotropic methyl $^1J_{CH}$ couplings were collected as previously described31. A similar sample in anisotropic medium containing 0.5 mM protein and 15 mg/mL filamentous pf1 phage (ASLA Biotech, Riga, Latvia) was used to measure PCB methyl RDCs ($^1D_{CH}$). 1-D ^{15}N-direct detected, 2-D ^{15}N-heteronuclear single quantum

coherence (HSQC), and ^{15}N NOE experiments used a 1 mM sample of unlabeled protein assembled with [*U*-^{15}N]-PCB31.

All NMR data were collected at 25 °C, except for the measurements of bicelle RDCs, which were collected at 33 °C. Distance constraints were obtained from 3-D ^{15}N-edited NOESY (t_{mix}=150 ms) and 3-D ^{13}C-edited NOESY (t_{mix}=120 ms) experiments. NH and $C^{\alpha}H^{\alpha}$ dipolar couplings were measured from a 3-D HNCO antiphase ^{1}H-coupled in the ^{15}N dimension34 and a 3-D HCA(CO)N antiphase ^{1}H-coupled in the ^{13}C dimension, respectively. PCB methyl RDCs were obtained from a J-modulated [^{1}H-^{13}C] HSQC spectrum35 recorded with a 600 MHz Bruker DMX-Avance spectrometer.

Resonance Assignments and Secondary Structure Calculations

^{15}N T_2 measurements with 1.7 mM [*U*-^{15}N; *U*-^{13}C]-*SyB*-Cph1(GAF) in Pr form yielded uniform values around 45 ms for the rigid part of the molecule31. Backbone assignments were obtained and assigned manually as described31. The TALOS program36 provided 152 pairs of φ/ψ backbone torsion angle restraints and identified the secondary structure, which was confirmed by local NOEs. Hydrogen bond restraints were inferred initially for α-helices and later for β-strands when the level of structural refinement allowed their unambiguous alignment within the β-sheet. Two distance restraints of 1.9 Å and 2.9 Å per involved pair of residues were used to represent hydrogen bonds for H^{N}-O and N-O, respectively37. To help assign NMR peaks to the Pr and Pfr forms, we classified them into three groups: peaks belonging to atoms with distinct Pfr assignments whose chemical shifts matched those determined previously for Pr, indicating that they correspond to the Pr component of the mixture31, peaks belonging to atoms without distinct Pfr assignments whose chemical shifts matched those for Pr, indicating that they correspond to atoms whose environment is unaffected by photoconversion, and peaks with chemical shifts different from those observed for Pr and thus unique to the Pfr form. Backbone signals within the three groups were extended to side chains by reference to NOE and HCCH-TOCSY spectra, and the three-group classification was updated manually.

For chromophore assignments, PCB synthesized with ^{15}N or ^{13}C-labelled ALA was used to unambiguously identify almost all protons, the ring D nitrogen, and carbonyl carbons based on NOE contacts among themselves and with unambiguously assigned protein protons. The only exceptions were the CH_2 moieties in the propionate chains, which are known to be mobile and not observable due to conformational broadening of their NMR signals. Protons 5-H, 15-H, 2-H, 3-H, 3′-H, and 18^1-CH_2 were assigned from ^{13}C-HSQC and ^{13}C-NOE spectra based on multiple NOE contacts with PCB methyls and by direct detection (Suppl. Fig. 2); their assignments were also confirmed by a multitude of intra PCB NOE contacts among themselves and with 2^1, 3^2, 7^1, 13^1 and 17^1 methyl groups. The proton and carbon assignments are in excellent agreement with NMR assignments of PCB published previously38,39.

3-D Structure Calculations and Refinements

Structure calculations and refinements made use of the torsion angle molecular dynamics and the internal variable dynamics modules of Xplor-NIH40. A separate structure

calculation run (100 conformers) was used to identify and generously constrain those side chain dihedral angles that exhibited a unique rotameric state in more than 90% of the conformers. PCB topologies and parameters were generated by the Dundee PRODRG2 Server41. Peak intensities in 3D NOESY spectra of the protein were assigned using the PIPP/STAPP package42 and converted into a continuous distribution of 1118 approximate interproton distance restraints, with a uniform 40% distance error applied to take into account spin diffusion. PCB distance restraints were obtained by classifying the NOE peak intensities into 3 bins (strong, medium, and weak) (Suppl. Fig. 7). We attempted to measure RDCs in more than one alignment medium. To accommodate consistent measurements at pH 8.5, hydrolysis-resistant dialkyl analogs43 of the traditional DMPC:DHPC bicelles were exploited44. Structural restraints were determined with negatively charged bicelle $^{1}D_{NH}$ and $^{1}D_{C\alpha H\alpha}$ RDC data. We also used as structural constraints the RDCs of the PCB methyls from protein aligned with pf1 phage. The $^{1}D_{NH}$ and $^{1}D_{C\alpha H\alpha}$ RDC sets measured in pf1 were used to obtain the protein alignment tensor in this medium, but not as direct structural constraints.

The final NMR structure for Pfr (PDB code 2KLI) and the further refined structure for Pr (PDB code 2KOI; original code 2K2N) do not include the C-terminal 6His tag and the first 30 amino acids. The Pr structure was improved by adding another set of protein NH and PCB methyl RDCs in negatively charged stretched gels and 187 ^{15}N and 131 ^{13}C additional protein NOEs. We also assigned additional PCB protons (5-H, 15-H, 2-H, 3-H, 3^{1}-H and 18^{1}-CH_2) and their associated NOE contacts with the protein and among themselves (44 new PCB NOEs), which resulted in a consistent tilted, out-of-place orientation of ring A in Pr. The new ensemble of refined Pr structures has an improved heavy atom root mean squared deviation over the structured backbone regions (0.30 Å from 0.43 Å) and a slightly improved agreement with all measured RDCs.

From 100 refined conformers, a subset of 20 low-energy conformers was selected to represent the Pr and Pfr solution structures. These Pr and Pfr conformers have a root mean square deviation of 0.30 Å and 0.44 Å for backbone heavy atoms over the most structured regions (residues 31–110, 136–171, and 183–202), respectively. The final set of conformers had no NOE constraint violations greater than 0.5 Å in more than 40% of the calculated models. PROCHECK45 analysis of the structured region in the 20 lowest energy Pfr conformers showed that 88.6% of the residues were within the most favored region, 11.3% in the allowed region, and 0.1% in the disallowed region of the Ramachandran map. A summary of the agreement between experimental constraints and calculated Pfr structures is provided in Supplemental Table 1.

Supplemental References

31. Cornilescu G, Ulijasz AT, Cornilescu CC, Markley JL, Vierstra RD. Solution structure of a cyanobacterial phytochrome GAF domain in the red-light-absorbing ground state. J. Mol. Biol. 2008; 383:403–413. [PubMed: 18762196]

32. Ulijasz AT, et al. Characterization of two thermostable cyanobacterial phytochromes reveals global movements in the chromophore-binding domain during photoconversion. J. Biol. Chem. 2008; 283:21251–21266. [PubMed: 18480055]

33. Ulmer TS, Ramirez BE, Delaglio F, Bax A. Evaluation of backbone proton positions and dynamics in a small protein by liquid crystal NMR spectroscopy. J. Am. Chem. Soc. 2003; 125:9179–9191. [PubMed: 15369375]
34. Cornilescu G, Bax A. Measurement of proton, nitrogen, and carbonyl chemical shielding anisotropies in a protein dissolved in a dilute liquid crystalline phase. J. Amer. Chem. Soc. 2000; 122:10143–10154.
35. Ottiger M, Delaglio F, Marquardt JL, Tjandra N, Bax A. Measurement of dipolar couplings for methylene and methyl sites in weakly oriented macromolecules and their use in structure determination. J. Magn. Reson. 1998; 134:365–369. [PubMed: 9761712]
36. Cornilescu G, Delaglio F, Bax A. Protein backbone angle restraints from searching a database for chemical shift and sequence homology. J. Biomol. NMR. 1999; 13:289–302. [PubMed: 10212987]
37. Wüthrich, K. NMR of Proteins and Nucleic Acids. Wiley Interscience; 1986.
38. Bishop JE, et al. Phycobiliprotein-bilin linkage diversity. I. Structural studies on A- and D-ring-linked phycocyanobilins. J. Biol. Chem. 1986; 261:6790–6796. [PubMed: 3084489]
39. Lagarias JC, Glazer AN, Rapoport H. Chromopeptides from C-phycocyanin. Structure and linkage of a phycocyanobilin bound to the beta subunit. J. Am. Chem. Soc. 1979; 101:5030–5037.
40. Schwieters CD, Kuszewski JJ, Tjandra N, Clore GM. The Xplor-NIH NMR molecular structure determination package. J. Magn. Reson. 2003; 160:65–73. [PubMed: 12565051]
41. Schuttelkopf AW, van Aalten DM. PRODRG: a tool for high-throughput crystallography of protein-ligand complexes. Acta Cryst. D Biol. Cryst. 2004; 60:1355–1363.
42. Garrett DS, Powers R, Gronenborn AM, Clore GM. A common sense approach to peak picking two-, three- and four-dimensional spectra using automatic computer analysis of contour diagrams. J. Magn. Reson. 1991; 95
43. Ottiger M, Bax A. Bicelle-based liquid crystals for NMR-measurement of dipolar couplings at acidic and basic pH values. J. Biomol. NMR. 1999; 13:187–191. [PubMed: 10070759]
44. Tjandra N, Bax A. Direct measurement of distances and angles in biomolecules by NMR in a dilute liquid crystalline medium. Science. 1997; 278:1111–1114. [PubMed: 9353189]
45. Laskowski RA, MacArthur MW, Moss DS, Thornton JM. PROCHECK: a program to check the stereochemical quality of protein structures. J. Appl. Cryst. 1993; 26:283–291.
46. Chenna R, et al. Multiple sequence alignment with the Clustal series of programs. Nucleic Acids Res. 2003; 31:3497–3500. [PubMed: 12824352]
47. Fischer AJ, et al. Multiple roles of a conserved GAF domain tyrosine residue in cyanobacterial and plant phytochromes. Biochemistry. 2005; 44:15203–15215. [PubMed: 16285723]
48. Oka Y, Matsushita T, Mochizuki N, Quail PH, Nagatani A. Mutant screen distinguishes between residues necessary for light-signal perception and signal transfer by phytochrome B. PLoS Genet. 2008; 4:e1000158. [PubMed: 18704165]
49. von Stetten D, et al. Highly conserved residues Asp-197 and His-250 in Agp1 phytochrome control the proton affinity of the chromophore and Pfr formation. J. Biol. Chem. 2007; 282:2116–2123. [PubMed: 17121858]
50. Wagner JR, et al. Mutational analysis of *Deinococcus radiodurans* bacteriophytochrome reveals key amino acids necessary for the photochromicity and proton exchange cycle of phytochromes. J. Biol. Chem. 2008; 283:12212–12226. [PubMed: 18192276]
51. Hahn J, et al. Probing protein-chromophore interactions in Cph1 phytochrome by mutagenesis. FEBS J. 2006; 273:1415–1429. [PubMed: 16689929]
52. Yang X, Stojkovic EA, Kuk J, Moffat K. Crystal structure of the chromophore binding domain of an unusual bacteriophytochrome, RpBphP3, reveals residues that modulate photoconversion. Proc. Natl. Acad. Sci. U.S.A. 2007; 104:12571–12576. [PubMed: 17640891]

References

1. Rockwell NC, Su YS, Lagarias JC. Phytochrome structure and signaling mechanisms. Annu. Rev. Plant Biol. 2006; 57:837–858. [PubMed: 16669784]

2. Vierstra, RD.; Karniol, B. Phytochromes in microorganisms. In: Briggs, WR.; Spudich, JL., editors. Handbook of Photosensory Receptors. Wiley-VCH Press; Weinheim, Germany: 2005. p. 171-196.
3. Essen LO, Mailliet J, Hughes J. The structure of a complete phytochrome sensory module in the Pr ground state. Proc. Natl. Acad. Sci. U.S.A. 2008; 105:14709–14714. [PubMed: 18799745]
4. Cornilescu G, Ulijasz AT, Cornilescu CC, Markley JL, Vierstra RD. Solution structure of a cyanobacterial phytochrome GAF domain in the red-light-absorbing ground state. J. Mol. Biol. 2008; 383:403–413. [PubMed: 18762196]
5. Wagner JR, Brunzelle JS, Forest KT, Vierstra RD. A light-sensing knot revealed by the structure of the chromophore-binding domain of phytochrome. Nature. 2005; 438:325–331. [PubMed: 16292304]
6. Wagner JR, Zhang J, Brunzelle JS, Vierstra RD, Forest KT. High resolution structure of *Deinococcus* bacteriophytochrome yields new insights into phytochrome architecture and evolution. J. Biol. Chem. 2007; 282:12298–12309. [PubMed: 17322301]
7. Yang X, Kuk J, Moffat K. Crystal structure of *Pseudomonas aeruginosa* bacteriophytochrome: photoconversion and signal transduction. Proc. Natl. Acad. Sci. U.S.A. 2008; 105:14715–14720. [PubMed: 18799746]
8. Quail PH. Phytochrome photosensory signalling networks. Nat. Rev. Mol. Cell Biol. 2002; 3:85–93. [PubMed: 11836510]
9. Rudiger W, Thummler F, Cmiel E, Schneider S. Chromophore structure of the physiologically active form (P(fr)) of phytochrome. Proc. Natl. Acad. Sci. U.S.A. 1983; 80:6244–6248. [PubMed: 16593380]
10. Kneip C, et al. Protonation state and structural changes of the tetrapyrrole chromophore during the Pr --> Pfr phototransformation of phytochrome: a resonance Raman spectroscopic study. Biochemistry. 1999; 38:15185–15192. [PubMed: 10563801]
11. Inomata K, et al. Sterically locked synthetic bilin derivatives and phytochrome Agp1 from *Agrobacterium tumefaciens* form photosensitive Pr- and Pfr-like adducts. J. Biol. Chem. 2005; 280:24491–24497. [PubMed: 15878872]
12. Inomata K, et al. Assembly of synthetic locked chromophores with *Agrobacterium* phytochromes Agp1 and Agp2. J. Biol. Chem. 2006; 281:28162–28173. [PubMed: 16803878]
13. Fodor SP, Lagarias JC, Mathies RA. Resonance Raman analysis of the Pr and Pfr forms of phytochrome. Biochemistry. 1990; 29:11141–11146. [PubMed: 2271702]
14. Yang X, Kuk J, Moffat K. Conformational differences between the Pfr and Pr states of *Pseudomonas aeruginosa* bacteriophytochrome. Proc. Natl. Acad. Sci. U.S.A. 2009 in press.
15. Ulijasz AT, et al. Characterization of two thermostable cyanobacterial phytochromes reveals global movements in the chromophore-binding domain during photoconversion. J. Biol. Chem. 2008; 283:21251–21266. [PubMed: 18480055]
16. Wagner JR, et al. Mutational analysis of *Deinococcus radiodurans* bacteriophytochrome reveals key amino acids necessary for the photochromicity and proton exchange cycle of phytochromes. J. Biol. Chem. 2008; 283:12212–12226. [PubMed: 18192276]
17. von Stetten D, et al. Highly conserved residues Asp-197 and His-250 in Agp1 phytochrome control the proton affinity of the chromophore and Pfr formation. J. Biol. Chem. 2007; 282:2116–2123. [PubMed: 17121858]
18. van Thor JJ, et al. Light-induced proton release and proton uptake reactions in the cyanobacterial phytochrome Cph1. Biochemistry. 2001; 40:11460–11471. [PubMed: 11560494]
19. Borucki B, et al. Light-induced proton release of phytochrome is coupled to the transient deprotonation of the tetrapyrrole chromophore. J. Biol. Chem. 2005; 280:34358–34364. [PubMed: 16061486]
20. Fischer AJ, et al. Multiple roles of a conserved GAF domain tyrosine residue in cyanobacterial and plant phytochromes. Biochemistry. 2005; 44:15203–15215. [PubMed: 16285723]
21. Karniol B, Wagner JR, Walker JM, Vierstra RD. Phylogenetic analysis of the phytochrome superfamily reveals distinct microbial subfamilies of photoreceptors. Biochem. J. 2005; 392:103–116. [PubMed: 16004604]

22. Oka Y, Matsushita T, Mochizuki N, Quail PH, Nagatani A. Mutant screen distinguishes between residues necessary for light-signal perception and signal transfer by phytochrome B. PLoS Genet. 2008; 4:e1000158. [PubMed: 18704165]

23. Rohmer T, et al. Light-induced chromophore activity and signal transduction in phytochromes observed by ^{13}C and ^{15}N magic-angle spinning NMR. Proc. Natl. Acad. Sci. U.S.A. 2008; 105:15229–15234. [PubMed: 18832155]

24. Seibeck S, et al. Locked 5*Zs*-biliverdin blocks the Meta-Ra to Meta-Rc transition in the functional cycle of bacteriophytochrome Agp1. FEBS Lett. 2007; 581:5425–5429. [PubMed: 17976380]

25. Inomata K, et al. Assembly of *Agrobacterium* phytochromes Agp1 and Agp2 with doubly locked bilin chromophores. Biochemistry. 2009; 48:2817–2827. [PubMed: 19253981]

26. van Thor JJ, Mackeen M, Kuprov I, Dwek RA, Wormald MR. Chromophore structure in the photocycle of the cyanobacterial phytochrome Cph1. Biophys. J. 2006; 91:1811–1822. [PubMed: 16751241]

27. Strauss HM, Hughes J, Schmieder P. Heteronuclear solution-state NMR studies of the chromophore in cyanobacterial phytochrome Cph1. Biochemistry. 2005; 44:8244–8250. [PubMed: 15938613]

28. Yang X, Stojkovic EA, Kuk J, Moffat K. Crystal structure of the chromophore binding domain of an unusual bacteriophytochrome, RpBphP3, reveals residues that modulate photoconversion. Proc. Natl. Acad. Sci. U.S.A. 2007; 104:12571–12576. [PubMed: 17640891]

29. Harper SM, Neil LC, Gardner KH. Structural basis of a phototropin light switch. Science. 2003; 301:1541–1544. [PubMed: 12970567]

30. Vreede J, Crielaard W, Hellingwerf KJ, Bolhuis PG. Predicting the signaling state of photoactive yellow protein. Biophys J. 2005; 88:3525–3535. [PubMed: 15722437]

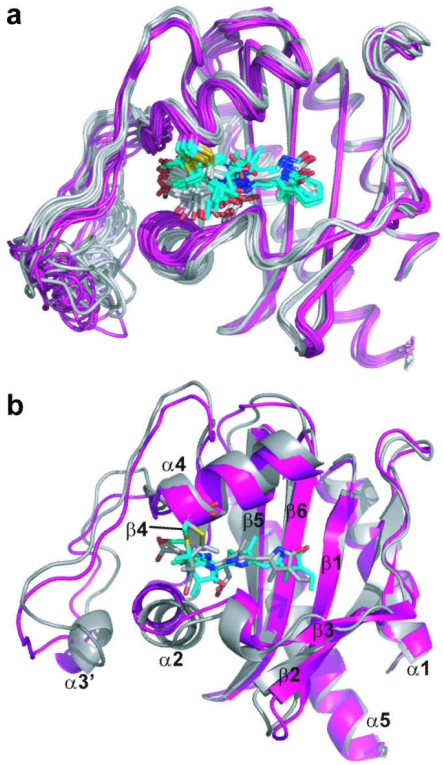

Figure 1. Three-dimensional overlay of *SyB*-Cph1(GAF) Pr and Pfr solution structures

The unstructured first 30 amino acids and C-terminal 6His-tag are not shown. **a,** Aligned Pr (grey) and Pfr (magenta) superimpositions of the protein backbone from their respective 20 lowest energy conformers. The PCB chromophore is shown in grey for Pr and cyan for Pfr. **b,** Same as **a**, but only the lowest energy conformer for Pr (grey) and Pfr (magenta) are shown. The α helices and β strands are labeled.

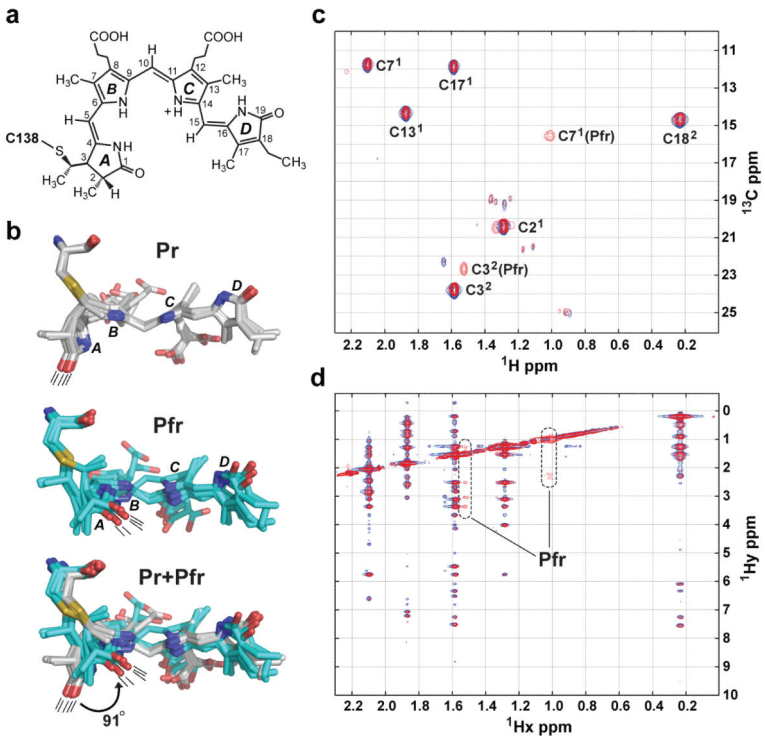

Figure 2. Rotation of the A ring of the PCB chromophore during Pr to Pfr photoconversion

a, Schematic diagram of PCB with numbered carbons for reference. **b,** Five lowest energy NMR conformers of PCB shown as a bundle in Pr (grey, top), Pfr (cyan, middle), and Pr/Pfr superimposition (bottom). The lines illustrate the direction of the A-ring carbonyl for each conformer. The indicated angle represents the Pr to Pfr rotation of the A ring for the lowest energy conformers. **c,** Two-dimensional ^{1}H-^{15}N heteronuclear single quantum coherence spectrum of *SyB*-Cph1(GAF) with ^{13}C incorporated into PCB carbons 2^{1} ,3^{2}, 7^{1}, 8^{2}, 12^{2}, 13^{1}, 17^{1}, and 18^{2} as Pr (blue) and following saturating red light irradiation (red, mixture of Pr and Pfr). **d,** Two-dimensional nuclear Overhauser effect spectrum of the sample in **c** showing ^{1}Hx/^{1}Hy crosspeaks from Pr (blue) and the mixture of Pr and Pfr (red). Only the $C3^{1}$ and $C7^{1}$ methyl carbons attached to PCB rings A and B (circled) show chemical shift changes upon photoconversion to Pfr whereas the chemical shifts for the $C13^{1}$, $C17^{1}$, $C18^{2}$ methyl carbons attached to the C and D rings are unaffected.

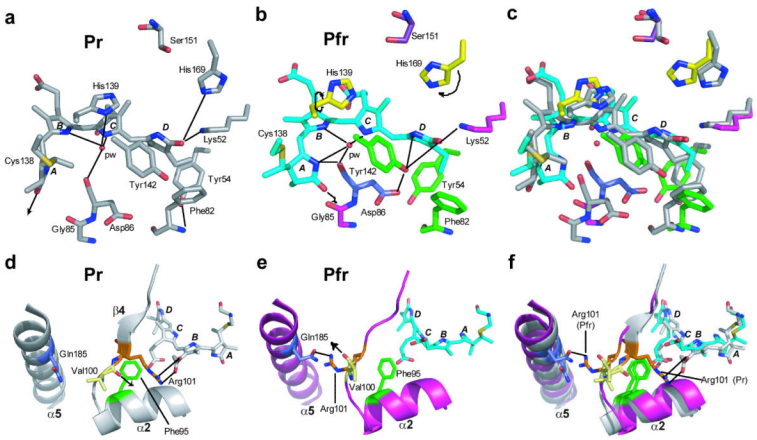

Figure 3. Light-driven conformational changes for amino acids surrounding the chromophore

a-c, Lowest energy structures for the PCB binding pocket as Pr (a), Pfr (b), and a superimposition of the two (c) highlighting conformational changes of relevant sidechains. The pyrrole water (pw) was modeled by aligning the available crystal structures for *Deinococcus radiodurans* BphP (PDB codes 1ZTU and 2O9B5,6) and *Synechocystis* Cph1 (PDB code 2VEA3) with the *SyB*-Cph1(GAF) solution structures. Straight arrows indicate the direction of the A-ring carbonyl of PCB in Pr and Pfr. Curved arrows indicate the directions of His139 and His169 sidechain movements. **d-f**, Ribbon representation for the region surrounding Arg101 as Pr (d), Pfr (e), and a superimposition of the two (f), highlighting the rotation of Val100 and Arg101 during photoconversion. Phe95 is shown in green, Val100 in yellow, Arg101 in orange, and Gln185 in purple. The 180° rotation of Val100 and Arg101 during Pr to Pfr photoconversion allows Arg101 to contact helix α5 at Gln185. Helix α2 and Phe95 move toward PCB to potentially block Arg101 from swiveling back to its Pr position. In all panels, the A-D pyrrole rings are indicated. Dashed lines highlight potential electrostatic interactions.

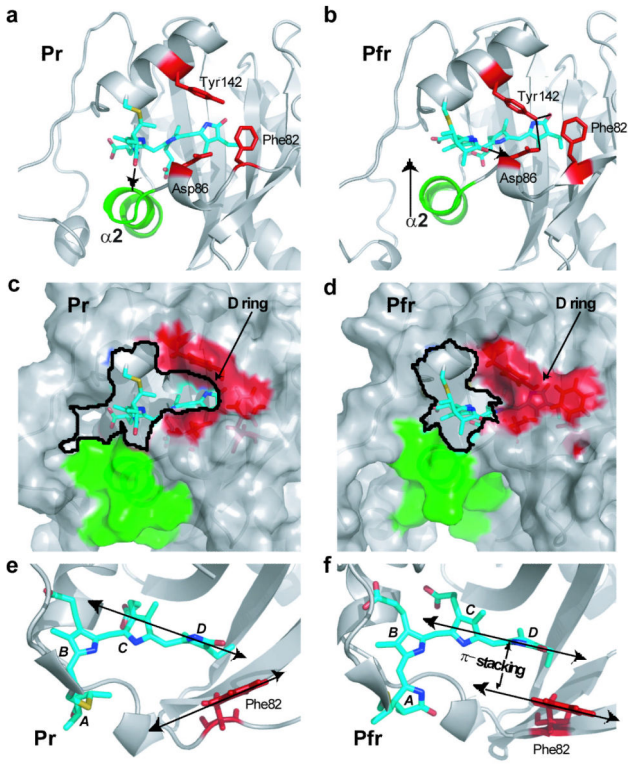

Figure 4. Conformational rearrangement of Asp86, Tyr142 and Phe82 during Pr to Pfr photoconversion

a and b, Ribbon representation of the structures of *SyB*-Cph1(GAF) as Pr (a) and as Pfr (b) illustrating the conformational changes combined with the upshift of helix α2 (green) during photoconversion. The small arrow indicates the orientation of the A-ring carbonyl. The large arrow in b highlights the displacement of helix α2. Proposed hydrogen bonds between Tyr142, Asp86 and the D ring nitrogen are indicated by the dashed lines. **c and d,** Changes in solvent accessibility for PCB in Pr (c) versus Pfr (d). The green and red areas show the solvent exposed surfaces of helix α2 and the Asp86/Tyr142/Phe82 triad, respectively. **e and f,** Predicted π-stacking of PCB with Phe82 (red) in the Pr (e) and Pfr states (f). Rotation of the aromatic ring of Phe82 upon Pfr formation generates a parallel displaced orientation that favors π stacking interactions with PCB. In all panels, PCB is shown in cyan, the A-D pyrrole rings are labeled, and the key amino acids are in red.